PIEZOELECTRICALLY TRANSDUCED HIGH-*Q* SILICA MICRO RESONATORS

Zhengzheng Wu[1], Adam Peczalski[1], Vikram A. Thakar[2], Zongliang Cao[1], Yi Yuan[1], Guohong He[1], Rebecca L. Peterson[1], Khalil Najafi[1], and Mina Rais-Zadeh[1,2]
[1]Electrical Engineering Department, University of Michigan, Ann Arbor, MI 48109, USA
[2]Mechanical Engineering Department, University of Michigan, Ann Arbor, MI 48109, USA

ABSTRACT

In this paper, we report on high-performance piezoelectric-on-silica micromechanical resonators for integrated timing applications. Fused silica is used as the resonator structural material for its excellent material properties, and thin film aluminum nitride is used as the piezoelectric transduction layer. A silica resonator is demonstrated with a high quality factor (Q_U ~25,841), low motional impedance (R_m ~350 Ω), and good power handling capability. The measured f×Q product of this resonator is the highest amongst reported micromachined silica/fused quartz resonators.

INTRODUCTION

Micromechanical (or MEMS) resonators are promising candidates as replacements for bulky quartz crystal frequency references. As compared to crystal oscillators (XTALs), MEMS resonators and oscillators provide an unprecedented level of miniaturization and integration. Most research has been focused on using silicon as the resonator body material and excellent performances have been obtained [1] [2]. In this work, fused silica is sought as a promising candidate for realizing high-Q micromechanical resonators because of its unique material properties. Excellent thermal isolation of fused silica makes it ideal as both the device and the packaging material, enabling all-silica packaged MEMS that can be oven controlled at low power. Such an ovenization scheme in a homogenous platform can be used to realize ultra-stable frequency sources [3]. Fused silica is also a material that has potentially very low intrinsic loss. In terms of phonon-phonon dissipation, a high f×Q product has been predicted for quartz [4], which has very similar material constants to silica. Fused silica or amorphous quartz has very low thermal conductivity and small linear expansion coefficient resulting in low thermoelastic damping (TED) [5]. TED could be the limiting factor in longitudinal mode resonators [5] and fused silica has the potential of exceeding the silicon performance at low frequencies where TED is a major Q limiting mechanism. Mechanical fused silica resonators with Qs exceeding a million have been demonstrated at kHz frequencies as early as 1970s [5]. However, despite its many exceptional material properties, research on micromachined silica resonators has not been very successful because of the fabrication limitations in defining high-aspect-ratio features and gaps in silica. Recently, capacitively transduced silica-on-silicon micro-resonators have been demonstrated, showing relatively high Qs but also a high level of insertion loss [6]. In this work, we choose piezoelectric actuation as it does not require small gaps for efficient transduction and devise a fabrication process to implement isolated silica resonators ideal for use in an all-silica platform [7]. The silica resonators in this work exhibit high Qs, low motional impedance, and good power handling capability. The resonator design, fabrication, and characterization results are discussed.

RESONATOR DESIGN

The silica resonator in this paper is an in-plane bulk mode resonator. As sketched in Figure 1, the resonator is comprised of two rings that are connected through a center coupling rod, which mimics a "dogbone" shape. The ring can vibrate in radial extensional mode. In this mode, the resonance frequency can be designed with lithographically defined geometries and is insensitive to the device thickness variation. The coupling rod is attached to the edge of the ring, which is a high velocity point for radial extensional mode. This creates a strong energy coupling between the two vibrating rings. The strong coupling splits the resonance frequencies of the in-phase and out-of-phase modes. The resonator is anchored at the center of the coupling rod, which is the *pseudo*-nodal point of the in-phase radial extension mode. Such an anchor structure avoids direct attachment to the vibrating rings, and, therefore, the in-plane radial extension mode has low anchor loss. The mechanical coupling scheme improves the power handling and reduces motional impedance compared to a single resonator [2]. As sketched in Figure 1, the drive and sense electrodes are placed on two rings to excite vibration. When an AC signal is applied across the piezoelectric layer on the drive electrode, mechanical strain (S) is induced through piezoelectric coupling coefficient (d_{31}). At resonance, vibration is effectively excited and the strain in the sense ring induces charge on the piezoelectric layer through reverse piezoelectric effect, which is picked up by the sense electrode. This realizes effective transduction between mechanical and electrical domains.

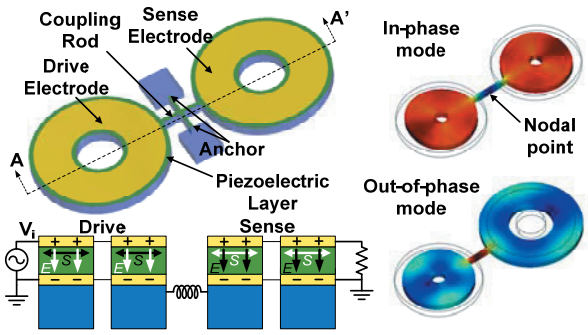

Figure 1. 3-D model of the silica resonator; diagram of piezoelectric actuation; and mode shapes of in-phase and out-of-plane coupled radial extensional mode.

RESONATOR FABRICATION

The fabrication process of the piezoelectric-on-silica resonator is sketched in Figure 2. The process starts with a 4" Corning 7980 high-purity fused silica wafer. A 1000 Å thick Molybdenum (Mo) layer is deposited and patterned as the bottom electrode. Then, a 1 µm thick Aluminum Nitride (AlN) layer is sputtered to form the piezoelectric material. The top electrode is formed by evaporation of a Cr/Au (100Å/1000Å) layer. The silica wafer is subsequently flipped and attached to a carrier for wafer thinning. Backside DRIE is used to define the resonator geometry [7]. Devices are detached from the carrier during the final release. The SEM image of a fabricated silica resonator is shown in Figure 3. The isolated silica resonator can be further capped and sealed using two additional silica layers to realize an all-silica packaged resonator with a very small form factor.

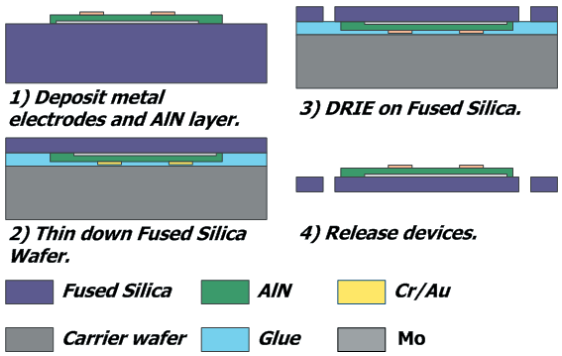

Figure 2. Fabrication process flow of the fused-silica resonators.

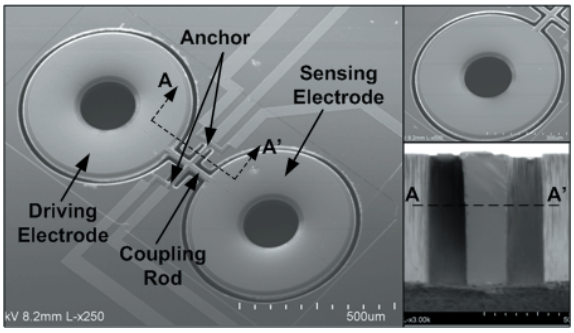

Figure 3. SEM images of the dogbone silica resonator and a cross-section showing the silica DRIE etch profile.

RESULTS AND ANALYSIS

Resonator Performance

The *S*-parameter responses of the resonators are measured using an Agilent E5061b vector network analyzer (VNA) at pressure levels below 1 mTorr. The silica resonator exhibits several distinctive vibration modes. Figures 4-6 plot the measured frequency responses of three vibration modes and their simulated mode shapes. A coupled in-plane shear mode is shown in Figure 4. This mode has a measured *Q* of 46,203 at 2.9 MHz. The top electrode geometry and placement could be optimized for this mode to achieve a better insertion loss. A high-*Q* in-plane radial breathing mode is plotted in Figure 5. This mode has a measured *Q* of 20,265 at 4.9 MHz with an insertion loss of 13.3 dB. The high-*Q* combined with low loss makes this mode ideal for making low-phase noise frequency sources. Another high-frequency second-order radial-extensional mode is captured at 16.4 MHz with a measured *Q* of ~ 3,325, as shown in Figure 6.

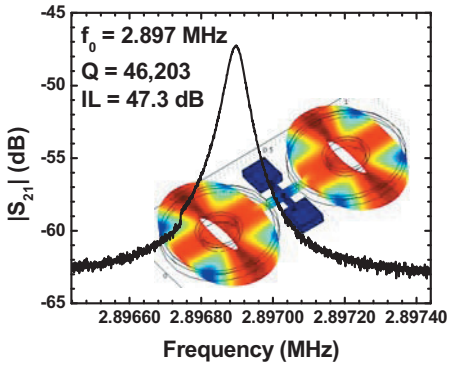

Figure 4. S-parameter response of the in-plane shear mode at 2.9 MHz.

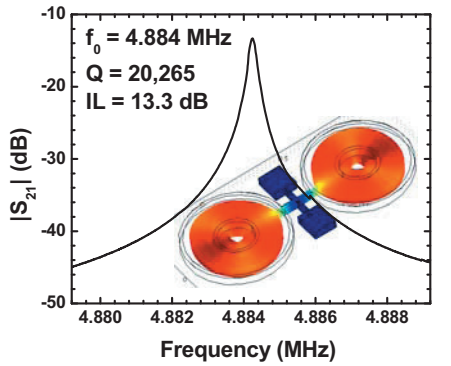

Figure 5. S-parameter response of the in-plane radial breathing mode at 4.9 MHz.

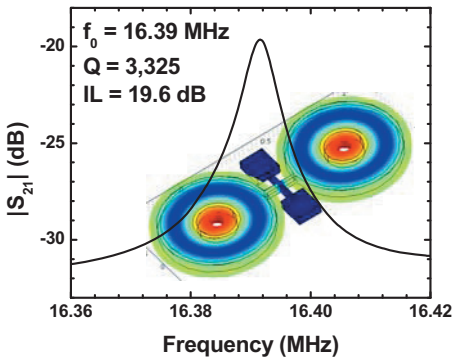

Figure 6. S-parameter response of the in-plane second-order radial-extensional mode at 16.4 MHz.

The above *Q*s are extracted from 3 dB fractional bandwidth of the measured transmission responses, $|S_{21}|$. Therefore, these *Q* values incorporate loading effects from the VNA 50Ω port impedances and other electrical parasitics. The unloaded *Q*-factor (Q_U), i.e. *Q* of the mechanical vibration mode, can be extracted after de-embedding the loading effects. As sketched in Figure 7, the measured device response is expressed by a two-port *Y*-parameter matrix, $[\mathbf{Y}_{\mathbf{DUT}}]$. The $[\mathbf{Y}_{\mathbf{DUT}}]$ incorporates a

network [$\mathbf{Y_{mech}}$], which accounts for piezoelectrically transduced mechanical vibration near resonance using a Butterworth-Van Dyke (BVD) model, and a network [$\mathbf{Y_{par}}$] which accounts for electrical parasitics. [$\mathbf{Y_{par}}$] can be obtained by fitting the measured wideband frequency response of the device to the parasitic model in Figure 7. The fitted parasitic model removes sharp mechanical resonance peaks. Therefore, the electrical parasitic network [$\mathbf{Y_{par}}$] incorporates only admittances Y_f, Y_{sub1}, and Y_{sub2}. Y_f accounts for the electrical feedthrough effect, including a feedthrough capacitance (C_f) and conductance (G_f). Y_{sub1} and Y_{sub2} in Figure 7 model the substrate effects, including the substrate parasitic capacitance (C_{sub1}, C_{sub2}) and parasitic conductance (G_{sub1}, G_{sub2}). The response of pure mechanical vibration [$\mathbf{Y_{mech}}$] can be obtained by subtracting the electrical parasitic network [$\mathbf{Y_{par}}$] from the measured device response [$\mathbf{Y_{DUT}}$]

$$[\mathbf{Y}_{\mathbf{mech}}] = [\mathbf{Y}_{\mathbf{DUT}}] - [\mathbf{Y}_{\mathbf{par}}], \quad (1)$$

and the S-parameter of the mechanical vibration [$\mathbf{S_{mech}}$] can be obtained from [$\mathbf{Y_{mech}}$]. At mechanical resonance, the motional impedance (R_m) can be extracted by

$$R_m = 2Z_0 S_{110} / (1 - S_{110}), \quad (2)$$

where S_{110} is the element from [$\mathbf{S_{mech}}$] matrix at mechanical resonance frequency. The coupling coefficient (k) is the ratio of the power dissipated by external loads to that dissipated by the unloaded resonator, and k can be extracted by

$$k = (1 - |S_{110}|) / |S_{110}|. \quad (3)$$

Finally, the unloaded Q-factor (Q_U) can be extracted as

$$Q_U = (1 + k) Q_L. \quad (4)$$

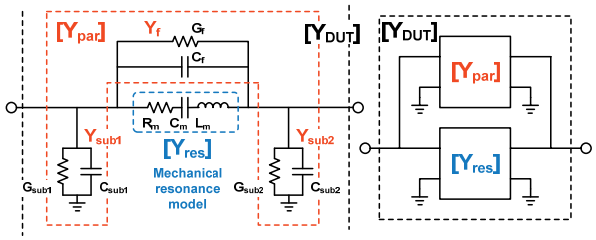

Figure 7. Y-parameter representation and equivalent circuit model of the resonator and electrical parasitics.

The Q_U extraction results for the silica resonator are summarized in Table 1. Here, the Q_U is the quality factor of the mechanical vibration with all the electrical loading effects de-embedded. The $f \times Q$ product demonstrated in this paper is the highest among reported micromachined fused silica/quartz resonators. The Q_{TED} for three modes are simulated using COMSOL commercial FEM package [8], and the results are summarized in Table 2. Also, a pure silica resonator with identical geometry is included for comparison in Table 2. It can be found that the pure silica resonator shows extremely high Q_{TED}. However, the AlN and metal electrode stack layers significantly increase the TED. This calls for improved designs, where the high thermal conductivity piezoelectric layer is patterned to reduce TED while maintaining a low insertion loss. Alternatively, one can use a lower thermal conductivity piezoelectric layer to achieve a higher Q. As seen from Tables 1 and 2, the measured Q is significantly lower than what the AlN-on-silica stack can offer. We believe the Q of the fabricated silica resonator is limited by anchor loss or surface loss mechanisms, which originate from structural asymmetry and non-ideal DRIE sidewall profiles, and can be further improved by optimizing the silica process.

Table 1: Extracted motional impedance (R_m), unloaded Q (Q_U), and f×Q product of the silica resonator.

Mode	R_m	Q_U	$f \times Q$
2.9 MHz	24.1 KΩ	46,394	1.35×10^{11}
4.9 MHz	357 Ω	25,841	1.27×10^{11}
16.4 MHz	1.33 KΩ	3,574	0.59×10^{11}

Table 2: Simulated Q_{TED} of three vibration modes for an AlN-on-silica resonator and a pure silica resonator.

Mode	*Silica with AlN/metal stack*	*Silica*
2.9 MHz	2.27×10^{5}	7.68×10^{9}
4.9 MHz	2.57×10^{5}	9.41×10^{10}
16.4 MHz	1.05×10^{5}	7.72×10^{10}

Nonlinearity and Power Handling

When making oscillators, power handling of the resonator is another important metric, as phase noise is inversely proportional to the driving power of the resonator [2]. Generally speaking, power handling of piezoelectric resonators is better than capacitive resonators as the nonlinearity due to capacitive transduction is not the limiting factor. To characterize the nonlinearity and power handling of the silica resonator, the frequency response of the resonator is measured under different source power levels, and the results are plotted in Figure 8. The measured $|S_{21}|$ responses show that there is high-frequency shift of the resonance peaks, indicating "spring stiffening" effect. Up to a source power of -3 dBm, instability is not observed. The actual power dissipated in sustaining the mechanical vibration (P_{drive}) is further extracted. By subtracting the reflected power back to the VNA and the power delivered to the load from the VNA source (P_{source}), the total power dissipated in the resonator (P_{diss}), i.e. the sum of mechanical and electrical power loss, is obtained. The P_{diss}/P_{source} ratio is plotted in Figure 9 for different source power levels. It can be observed that there is maximum mechanical power dissipation at the resonance frequency, which is also the zero phase transition of the resonator phase response. The power driving the mechanical vibration (P_{drive}) is also listed in Figure 9.

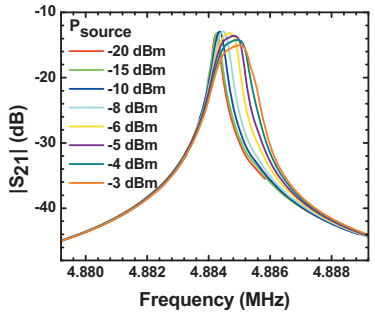

Figure 8. S-parameter responses of the 4.9 MHz resonance mode with various source power levels.

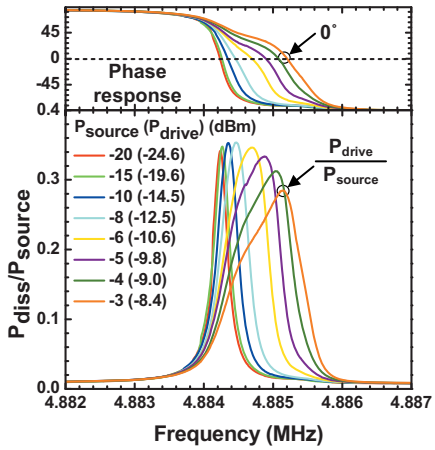

Figure 9. The ratio of dissipated power to source power (P_{diss}/P_{source}) for the 4.9 MHz mode at various source power levels and the extracted resonator driving power (P_{drive}).

Temperature Sensitivity

The temperature coefficient of frequency (TCF) of the silica resonator is characterized across -40˚C to +85˚C. The resonance frequency is measured in a temperature -controlled probe station, and the results are plotted in Figure 10. The TCF values for three vibration modes are extracted using a linear model. The extracted first-order TCF values range from +76 to +90 ppm/˚C. The higher TCF value compared with silicon resonators is mainly due to the intrinsic material property of fused silica, i.e. higher temperature coefficient of Young's Modulus. In order to make a temperature stable timing reference, TCF of silica resonators can be reduced using passive material compensation. A higher stability can be achieved by a ovenizing the all-silica platform [3], where the excellent thermal and isolation properties of silica are fully utilized.

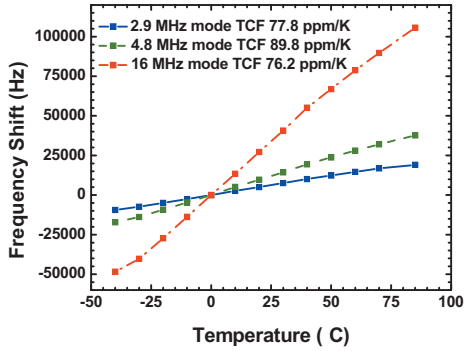

Figure 10. Resonator frequency shift versus temperature and extracted TCF for three vibration modes.

Silica vs. Silicon

In Table 3, the fused silica resonator of this work is benchmarked against reported silicon MEMS resonators that showed high *Q*s and low motional impedances. As shown, the micromachined silica resonator has comparable performance to silicon resonators. Further improvement in silica micromachining process can have a significant impact in improving the silica device performance. Also, developed techniques for silicon can be extended to silica to implement high-performance silica-based oscillators.

Table 3: Comparison of MEMS resonators.

Resonator	*Material*	*Q*	R_m (V_p)
60 MHz [2]	Si (capacitive)	118,900	2.6 KΩ (7V)
6 MHz [9]	Si (capacitive)	39,000	218 Ω (18V)
1 MHz [10]	AlN-on-Si	140,000	200 Ω
36 MHz [1]	AlN-on-Si	17,000	180 Ω
This work	**AlN-on-silica**	**25,841**	**357 Ω**

CONCLUSION

In this paper, a piezoelectric-on-silica resonator is reported that exhibits high *Q*, low motional impedance, and good power handling capability. This is the first step towards the implementation of an all-silica timing platform leveraging excellent thermal and acoustic properties of fused silica.

ACKNOWLEDGEMENTS

This work was supported by DARPA under Single-chip Timing and Inertial Measurement Unit (TIMU) program, award #N66001-11-C-4170. The authors would like to acknowledge the staff at Michigan Lurie Nanofabrication Facilities (LNF).

REFERENCES

[1] R. Abdolvand, H. Lavasani, G. Ho, F. Ayazi "Thin-film piezoelectric-on-silicon resonators for high-frequency reference oscillator applications," *IEEE Trans. Ultrason. Ferroelect., Freq. Contr.,* vol. 55, no. 12, pp. 2596-2606, Dec. 2008.

[2] Y.-W. Lin, S.-S. Li, Z. Ren, C.T.C. Nguyen, "Low phase noise array-composite micromechanical wine-glass disk oscillator," *Tech. Dig. IEEE IEDM 2005*, pp. 4 pp. -281, Dec. 2005.

[3] J. C. Salvia, *et al.*, "Real-time temperature compensation of MEMS oscillators using an integrated micro-oven and a phase-locked loop," *J. Microelectromech. Syst.*, vol. 19, no. 1, pp. 192-201, Feb. 2010.

[4] R. Tabrizian, M. Rais-Zadeh, F. Ayazi, "Effect of phonon interactions on limiting the *f*·*Q* product of micromechanical resonators," *Proc. TRANSDUCERS 2009*, pp. 2131-2134, 21-25, June 2009.

[5] Braginskiĭ, V. B, V. P Mitrofanov, *Systems with Small Dissipation*, University of Chicago Press, 1985.

[6] Y.-S. Hwang, *et al.*, "Fabrication of electrostatically -actuated, in-pane fused quartz resonators using silicon-on-quartz (SoQ) bonding and quartz DRIE," *Proc. IEEE MEMS 2009*, pp. 729-732, Jan. 2009.

[7] Z. Cao, *et al.*, "DRIE of fused silica," *Proc. MEMS 2013*.

[8] A. Duwel, R. N. Candler, T. W. Kenny, M. Varghese, "Engineering MEMS resonators with low thermoelastic damping," *J. Microelectromech. Syst.*, vol. 15, no. 6, pp. 1437-1445, Dec. 2006.

[9] G. K. Ho, *et al.*, "Micromechanical IBARs: tunable high-*Q* resonators for temperature-compensated reference oscillators," *J. Microelectromech. Syst.*, vol. 19, no. 3, pp. 503-515, June 2010.

[10] J. Baborowski, *et al.*, "Piezoelectrically activated silicon resonators," *Proc. IEEE IFCS 2007,* pp. 1210-1213, May 2007.